Published on 27 November 2015. Downloaded by RESEARCH CENTRE FOR ECO-ENVIRONMENTAL SCIENCES, CAS on 23/02/2016 08:39:49.

PCCP

PAPER

View Article Online
View Journal | View Issue

Cite this: *Phys. Chem. Chem. Phys.*, 2016, **18**, 956

Synergistic formation of sulfate and ammonium resulting from reaction between SO_2 and NH_3 on typical mineral dust†

Weiwei Yang, Hong He,* Qingxin Ma, Jinzhu Ma, Yongchun Liu, Pengfei Liu and Yujing Mu

Received 12th October 2015,
Accepted 27th November 2015

DOI: 10.1039/c5cp06144j

www.rsc.org/pccp

The heterogeneous reactions of SO_2 and NH_3 on typical mineral oxides were investigated using *in situ* diffuse reflectance infrared Fourier transform spectroscopy (DRIFTS). A new sulfate formation pathway was proposed where NH_3 accelerated the formation of sulfate species. The results revealed that surface hydroxyls and oxygen played principal roles in the conversion of SO_2 to sulfate. It was proposed that NH_3 adsorbed onto Lewis acid sites, and hydroxyls and water molecules adsorbed on the surfaces of mineral dust. The enhancement of surface Lewis basicity by NH_3 induced more SO_2 molecules to adsorb on the surface, which were further oxidized to sulfate by interacting with surface hydroxyls and oxygen atoms. The formation of sulfate, in turn, contributed to the adsorption of NH_3, mainly as NH_4^+ due to enhanced Brønsted acid sites. The IC results showed that the synergistic effect between SO_2 and NH_3 was more significant on acidic oxides like γ-Al_2O_3 and α-Fe_2O_3 compared to basic oxides like MgO.

Introduction

Sulfur dioxide (SO_2) is a major anthropogenic pollutant in the atmosphere, which contributes to the formation of sulfuric acid and sulfate aerosols and then haze. Atmospheric sulfate particles are known to affect the radiation balance by scattering light and influence the properties of clouds by acting as cloud condensation nuclei (CNN).[1,2] SO_2 can be converted to secondary sulfate aerosols through homogeneous and heterogeneous pathways. Homogeneous (*i.e.* gas-phase) oxidation of SO_2 is dominated by the reaction with hydroxyl radicals followed by condensation into sulfuric acid in the presence of water vapor.[3] Recent laboratory and field studies have also highlighted the potential importance of Criegee intermediates (CIs) in tropospheric sulfate formation.[4,5] Aqueous-phase oxidation of dissolved SO_2, dominated by hydrogen peroxide and ozone, is probably the most important heterogeneous reaction pathway in cloudwater.[6,7] Other atmospheric oxidants, such as organic peroxides, oxygen, OH radicals, and nitrogen dioxides, may also result in a high level of sulfate formation in aqueous reaction.[8] An additional pathway involved in the transformation of SO_2 to sulfate particles is related to heterogeneous reactions of SO_2 on sea-salt aerosols and mineral dust.[9,10] Heterogeneous reactions on solids have been reported to play an important role in determining the composition of the gaseous troposphere.[11] An annual average of 50% to 70% of total sulfate is calculated to be associated with mineral dust in the vicinity of the dust source regions.[12,13] It was suggested that the in-cloud oxidation of SO_2 catalyzed by natural metal ions on mineral dust should be included in applied models, in which atmospheric SO_2 concentrations are typically overestimated and sulfate concentrations tend to be underestimated.[14] For instance, aqueous oxidation of SO_2 with oxygen was not negligible when catalyzed by Fe(III) and Mn(II) under high-pH conditions.[8] These results implied that heterogeneous conversion of SO_2 to sulfate on mineral dust may make an important contribution to sulfate formation.

Up to now, a number of mechanisms concerning heterogeneous reactions of SO_2 on mineral dust have been proposed where the adsorption of SO_2 only leads to sulfite or bisulfite on the surface of mineral oxides other than iron oxides and magnesium oxide.[15–20] Oxidants, such as O_3 and NO_2, are needed in the conversion of sulfite to sulfate.[20–23] Recently, He *et al.* reported that the coexistence of NO_x and SO_2 can lead to a rapid conversion of SO_2 to sulfate, combining laboratory studies and field measurements.[24] Another study by Kong *et al.* found

State Key Joint Laboratory of Environment Simulation and Pollution Control, Research Center for Eco-Environmental Sciences, Chinese Academy of Sciences, Beijing 100085, China. E-mail: honghe@rcees.ac.cn; Fax: +86-10-62849123; Tel: +86-10-62849123

† Electronic supplementary information (ESI) available: The physical properties of mineral oxides; the IC results of the amount of sulfate and ammonium formed on α-Fe_2O_3 with different exposure times to SO_2 or/and NH_3 in the *in situ* chamber; XRD of mineral oxides; DRIFTS spectra for adsorption of SO_2 on γ-Al_2O_3 followed by exposure to O_3; DRIFTS spectra of TiO_2 and MgO exposed to SO_2 or/and NH_3; Raman spectra of TiO_2 pristine and calcined at 500 °C for 20 h in air. Comparison of surface products formed on calcined-TiO_2 and fresh-TiO_2. See DOI: 10.1039/c5cp06144j

This journal is © the Owner Societies 2016

Published on 27 November 2015. Downloaded by RESEARCH CENTRE FOR ECO-ENVIRONMENTAL SCIENCES, CAS on 23/02/2016 08:39:49.

that surface nitrate on hematite participated in the heterogeneous reaction of SO_2 and accelerated the formation of sulfate.[25] However, there remain large uncertainties regarding the interaction mechanisms between SO_2 and minerals; for example, in the laboratory studies, little attention has been paid to the effects of other species (such as NH_3) on the heterogeneous reactions of SO_2. As is known, NH_3 is the most important basic gas in the atmosphere, with global emissions greater than 33 Tg nitrogen per year.[26] It participates as NH_4^+ in the formation of secondary particulate matter through the neutralization of HNO_3 and H_2SO_4.[27,28] Theoretical and experimental studies found that NH_3 addition promoted the nucleation and growth of sulfate aerosols in the ternary H_2SO_4–H_2O–NH_3 system.[29,30] Early studies have found that ammonia can accelerate the oxidation of SO_2 to sulfate in the thin film of water on vessel surfaces or on the skin of water droplets nucleated by soot or NaCl aerosols, and that the conversion was only dependent on the water content of aerosol.[31,32] However, mineral dust is different relative to vessel surfaces, soot and NaCl, because the surface of an oxide is usually covered by different kinds of hydroxyl groups and oxygen defects, whereby mineral particles can provide reactive surfaces to adsorb and catalyze reactions of trace gases in the atmosphere.[33–35] Given the difference in physicochemical nature, it is necessary to explore the effect of NH_3 on the heterogeneous reactions of SO_2 on different types of mineral dust.

In this study, heterogeneous reactions of SO_2 and NH_3 on typical mineral oxides (γ-Al_2O_3, TiO_2, MgO, and α-Fe_2O_3) were investigated and possible mechanisms for SO_2 oxidation and synergistic reactions between SO_2 and NH_3 on mineral oxides were elucidated.

Experimental section

Materials

The γ-Al_2O_3, TiO_2 (anatase), and MgO particles used in this study were purchased from commercial sources, while α-Fe_2O_3 was prepared using a precipitation method as reported.[36] The nitrogen adsorption–desorption isotherms of mineral oxides were obtained at 77 K over the whole range of relative pressures using a Quantachrome Quadrasorb SI-MP system. The results are listed in Table S1 (ESI†). X-ray diffraction (XRD) equipped with a Cu Kα (λ = 0.15406 nm) radiation source was applied to characterize the samples on a computerized PANalytical X'Pert Pro diffractometer system (Fig. S1, ESI†). The specifications of the gases used in this experiment are as follows: SO_2 (0.25% in N_2, Beijing Huayuan), NH_3 (0.20% in N_2, Beijing Huayuan), N_2 and O_2 (99.999% purity, Beijing Huayuan).

Experimental methods

In situ DRIFTS

In situ DRIFTS spectra were recorded on a Nicolet Nexus 670 FTIR equipped with a mercury cadmium telluride (MCT) detector, ranging from 4000 to 600 cm^{-1} at a resolution of 4 cm^{-1} for 100 scans. Before experiments, oxide samples were finely ground and placed into a ceramic crucible in the *in situ* chamber. All of the samples were pretreated at room temperature (303 K) and pressure for 120 min to remove adsorbed species in a stream of synthetic air (80% N_2 and 20% O_2) in a total flow of 100 mL min^{-1}, and then the samples were exposed to 200 ppmv SO_2 and/or 100 ppmv NH_3 balanced with 100 mL min^{-1} synthetic air.

XPS

X-ray photoelectron spectroscopy (XPS) with Al Ka radiation (1486.7 eV) was used to analyze the atomic state of adsorbed species on the surface of the sample (Axis Ultra, Kratos Analytical Ltd). The C 1s peak at 284.6 eV was used as an internal standard for peak position measurements.

IC

The products formed on the samples were analyzed by means of ion chromatography. To prevent sulfite oxidation, the reacted particles were protected with 15% formaldehyde before dilution with ultrapure water to 10 mL (specific resistance $\geq$18.2 MΩ cm) and then extracted by sonication for 30 min. The leaching solution was obtained through a 0.22 μm PTFE membrane filter and then was analyzed using Wayee IC-6200 ion chromatography equipped with a TSKgel Super IC-CR cationic or a SI-524E anionic analytical column. An eluent of 3.5 mM Na_2CO_3 was used at a flow rate of 0.8 mL min^{-1}. All of the measurements were repeated at least three times.

Results and discussion

Heterogeneous reactions of SO_2 and NH_3 on γ-Al_2O_3

Fig. 1 shows the *in situ* DRIFTS spectra of γ-Al_2O_3 exposed first to SO_2 and then NH_3 (Fig. 1(A)) or the reverse order (Fig. 1(B)) in synthetic air as a function of time. Upon SO_2 adsorption (Fig. 1(A)), three bands attributed to SO_2-chemisorbed species at 1225, 1080 and 964 cm^{-1} were readily observed. The bands at 1080 and 964 cm^{-1} are commonly assigned to the stretching modes of adsorbed sulfite or bisulfite on the surface of oxides.[15,18,37,38] An early study observed a weak SO_2 adsorption at 1210–1230 cm^{-1} on Na-doped γ-Al_2O_3 and explained that this band was due to the presence of sodium sulfite.[19] To confirm the surface bound species at 1225 cm^{-1}, the chemisorbed SO_2 on γ-Al_2O_3 was further oxidized with ozone as reported by Usher *et al.*[20] (Fig. S2, ESI†). With increased exposure time to O_3, the band at 1225 cm^{-1} grew rapidly, indicating that the band at 1225 cm^{-1} can be assigned to sulfate species.

After being pre-saturated by SO_2, the sample was subsequently purged by N_2 for 120 min and then the gas flow was switched to NH_3. As the exposure time increased, new bands at 1461 and 1267 cm^{-1} and a broad adsorption band between 3400 and 2700 cm^{-1}, with features at 3344, 3201, 3031, and 2784 cm^{-1}, were detected. The band at 1267 cm^{-1} was due to the symmetric deformation of NH_3 ($\delta_s(NH_3)$) coordinatively bound to Lewis acid sites; correspondingly, the bands in the

Published on 27 November 2015. Downloaded by RESEARCH CENTRE FOR ECO-ENVIRONMENTAL SCIENCES, CAS on 23/02/2016 08:39:49.

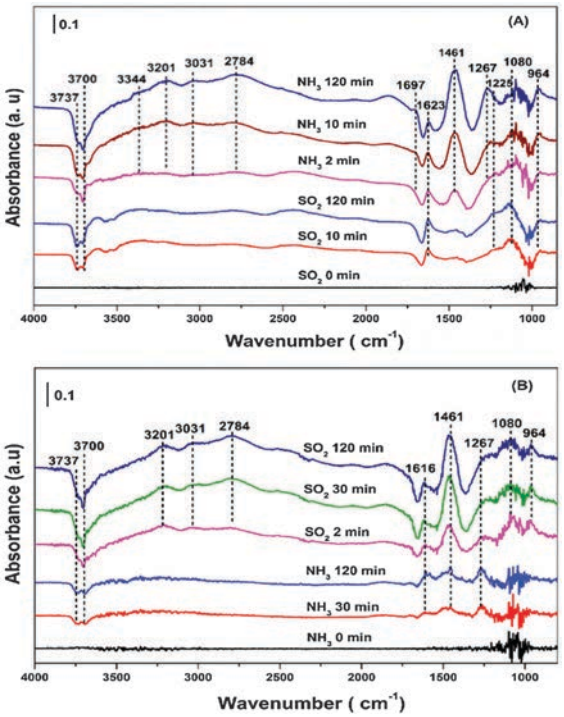

Fig. 1 *In situ* DRIFTS spectra of (A) 200 ppmv SO_2 reaction on the γ-Al_2O_3 surface followed by 100 ppmv NH_3 reaction; (B) 100 ppmv NH_3 reaction on the γ-Al_2O_3 surface followed by 200 ppmv SO_2 as a function of time in a flow of 100 mL min^{-1} synthetic air (80% N_2 and 20% O_2) at 303 K.

N–H stretching region were also observed at 3201 cm^{-1} ($\nu_s(NH_3)$) and 3344 cm^{-1} ($\nu_{as}(NH_3)$).[39–41] The bands at 1697 and 1461 cm^{-1} were assigned to the symmetric ($\delta_s(NH_4^+)$) and asymmetric ($\delta_{as}(NH_4^+)$) deformation of NH_4^+ bound on Brønsted acid sites corresponded to broad adsorptions at 3031 and 2784 cm^{-1} ($\nu(NH_4^+)$).[42,43] It was noted that the band at 1225 cm^{-1} attributed to sulfate species was overlapped by the band of 1267 cm^{-1} ($\delta_s(NH_3)$), thus no observable effect of NH_3 on sulfate formation was detected.

In Fig. 1(B), the sample was first exposed to NH_3 for 120 min in synthetic air flow, followed by N_2 purge, and then SO_2 was introduced to the gas flow. In contrast to Fig. 1(A), NH_3 adsorption at 1616 ($\delta_{as}(NH_3)$), 1461 ($\delta_{as}(NH_4^+)$) and 1267 cm^{-1} ($\delta_s(NH_3)$) was weak even after a 120 min reaction. The results implied that the pre-sorption of SO_2 promoted the adsorption of NH_3 on γ-Al_2O_3. Once the sample was exposed to SO_2, chemisorbed SO_2 species at the bands of 1225, 1080 and 964 cm^{-1} were detected. After SO_2 was introduced onto the surface of the sample, bands of NH_4^+ bound to Brønsted acid sites at 3031, 2784 ($\nu(NH_4^+)$) and 1461 cm^{-1} ($\delta_{as}(NH_4^+)$) grew in intensity as the exposure time increased. It was likely that NH_3 adsorbed on Lewis acid sites transformed into NH_4^+ in the presence of SO_2. The results further implied that SO_2 had a positive effect on the formation of NH_4^+ on γ-Al_2O_3. In contrast, no obvious effect of NH_3 on the formation of sulfate species was observed due to the poor signal from 1200 to 900 cm^{-1}.

To further study the influence of the gaseous reactants on each other in the heterogeneous reaction on γ-Al_2O_3, SO_2 and

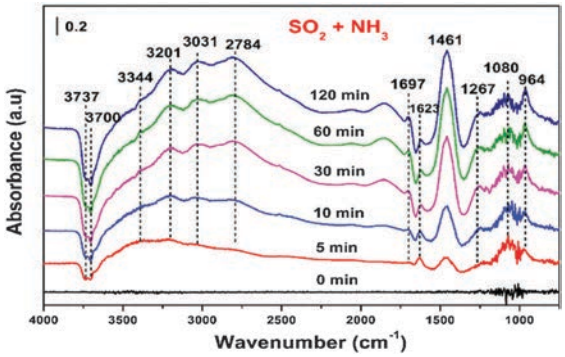

Fig. 2 Dynamic changes in the *in situ* DRIFTS spectra of γ-Al_2O_3 as a function of time with a flow of 200 ppmv SO_2 + 100 ppmv NH_3 + 20% O_2 + 80% N_2 at 303 K.

NH_3 were introduced simultaneously, and the DRIFTS spectra are shown in Fig. 2. It was obvious that adsorbed NH_3 species rapidly dominated on the surface of γ-Al_2O_3. Meanwhile, the formation of sulfite species was clearly observed at bands of 1080 and 964 cm^{-1}. Compared to the individual reaction of SO_2 or NH_3 on γ-Al_2O_3 in Fig. 1, more chemisorbed NH_3 and SO_2 species formed on the surface of the sample. To clearly illustrate the interaction between SO_2 and NH_3, the integrated areas of bands at 964 and 1461 cm^{-1} attributed to sulfite and ammonium in Fig. 1 and 2 were compared as shown in Fig. 3. Compared to the individual gaseous reactant reactions, sulfite and ammonium increased significantly in the reaction when SO_2 and NH_3 coexisted. Therefore, a synergistic effect between SO_2 and NH_3 existed on the surface of γ-Al_2O_3.

Since the DRIFTS spectra cannot clearly identify the sulfate species formed on γ-Al_2O_3, XPS was used to confirm the chemical speciation of surface-adsorbed species (Fig. 4). In Fig. 4(A), the S 2p spectrum showed two peaks with binding energies at 168.5 ± 0.2 eV and 169.5 ± 0.3 eV for S $2p_{3/2}$ by fitting the experimental photoelectron peaks. The former was assigned to the S–O band in SO_3^{2-} species and the latter was due to the presence of SO_4^{2-}.[18,44] It is obvious that sulfite was the dominant species on the surface regardless of the presence of NH_3. In Fig. 4(B), the N 1s spectra exhibited a main peak at

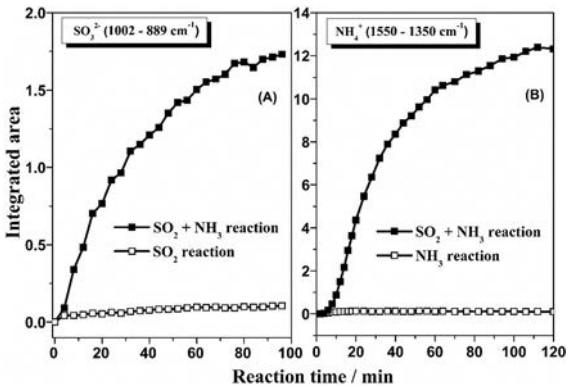

Fig. 3 Comparison of the integrated absorbance area for (A) sulfite and (B) ammonium under different reaction conditions.

This journal is © the Owner Societies 2016

Published on 27 November 2015. Downloaded by RESEARCH CENTRE FOR ECO-ENVIRONMENTAL SCIENCES, CAS on 23/02/2016 08:39:49.

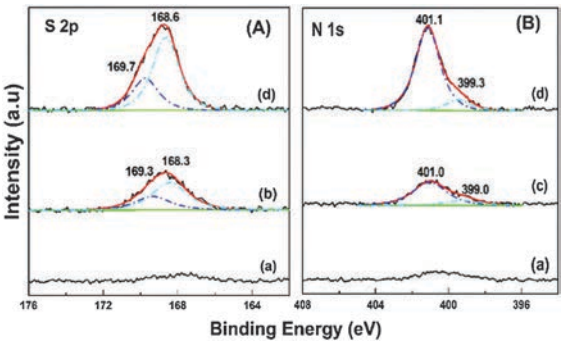

Fig. 4 XPS spectra of (A) S 2p and (B) N 1s, (a) fresh γ-Al_2O_3, (b) treated by individual 200 ppmv SO_2, (c) individual 100 ppmv NH_3, and (d) 200 ppmv SO_2 and 100 ppmv NH_3 simultaneously balanced with synthetic air in a flow of 100 mL min^{-1} for 120 min followed by purging N_2.

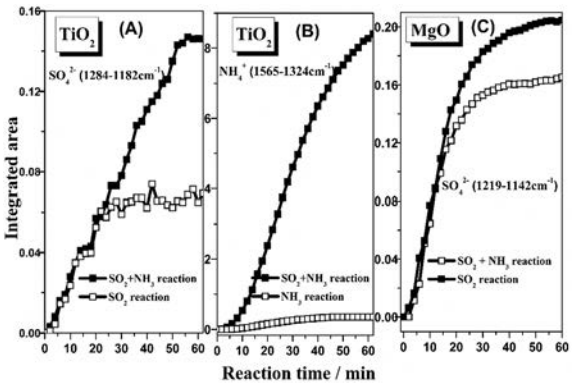

Fig. 5 Comparison of the integrated absorbance area for sulfate and ammonium under different reaction conditions.

401.0 $\pm$ 0.1 eV with a shoulder at 399.0 $\pm$ 0.3 eV ascribed to NH_4^+ bound on Brønsted acid sites and NH_3 chemisorbed on Lewis acid sites, respectively.[45] Similar to the IR results, sulfite and ammonium also increased in amount after treatment with SO_2 and NH_3 simultaneously compared to that after treatment with SO_2 or NH_3 individually, further supporting that SO_2 and NH_3 react on γ-Al_2O_3 synergistically.

Heterogeneous reactions of SO_2 and NH_3 on other typical mineral oxides

To clarify whether the synergistic effect between SO_2 and NH_3 existed on other typical mineral oxides, *in situ* DRIFTS experiments were also carried out on TiO_2, MgO and α-Fe_2O_3. DRIFTS spectra are shown for TiO_2, MgO and α-Fe_2O_3 in Fig. S3 and S4 (ESI†) and Fig. 6, respectively. The assignments of surface species formed during the reactions are summarized in Table 1. The SO_2 or/and NH_3 reactions on TiO_2 and MgO were similar except for the weak adsorption of NH_3 on MgO. Both sulfite and sulfate species formed on the surfaces when SO_2 reacted alone. For the NH_3 reaction, only weakly adsorbed NH_3 coordinated on Lewis acid sites was observed for MgO; the coverage of NH_4^+ on TiO_2 was low due to no observation of its vibration modes in the high N–H stretching region.[39,42] When SO_2 and NH_3 coexisted in the gas flow, NH_3 on Lewis acid sites was clearly transformed to NH_4^+ bound on Brønsted acid sites. For TiO_2, sulfite species decreased while the transformation of bridging sulfate to bidentate sulfate was observed, indicating that sulfate species concentrated on the surface of TiO_2. According to the integrated areas (Fig. 5), a synergistic reaction between SO_2 and NH_3 existed on TiO_2 and MgO.

The oxide α-Fe_2O_3 was slightly different relative to other oxides because it is reactive in the conversion of SO_2 towards sulfate at room temperature. When α-Fe_2O_3 was exposed to SO_2 (Fig. 6(A)), bands at 1248, 1168 and 1024 cm^{-1} attributed to bidentate sulfate grew in intensity with increased exposure time.[46,47] The bands at 1338 and 1318 were also observed by other researchers, possibly due to the accumulation of sulfate species.[25,47–49] In the case of NH_3 reaction, only weak adsorption of NH_3 coordinated on Lewis acid sites was observed.[39] When the sample was exposed to SO_2 and NH_3 simultaneously (Fig. 6(B)), a band at 1109 cm^{-1} appeared and the bands at 1318, 1248 and 1165 cm^{-1} red-shifted slightly. In addition, new bands at 3212, 3036, 2842 and 1434 cm^{-1} derived from chemisorbed NH_3 were observed.[42] The results indicated that a different situation occurred in the presence of SO_2 and NH_3.

Previous studies found that the conversion of monodentate into bidentate sulfate was favored during acidification and that the stretching frequency would increase in this process, regardless of the wet or dry state.[47,54] Persson *et al.* observed

Table 1 Vibrational frequencies of chemisorbed species formed on the surfaces of mineral dust

Surface species		γ-Al_2O_3	TiO_2	MgO	α-Fe_2O_3
SO_3^{2-}/HSO_3^-		1080, 964[15,19]	1087[23,50]	1043, 958[15,20,23]	
SO_4^{2-}	Bridging		1209, 1133[23,50–52]		1290, 1240, 1156, 1024[53–55]
	Bidentate	1225[18,20]	1245[23,50,51]	1198, 1167[15,23,56,57]	1248, 1168, 1024[16,46–48,58]
L-acid sites	$\delta_{as}(NH_3)$	1616[39–41,43]	1587, 1546[59–61]	1611[39]	1604[39]
	$\delta_s(NH_3)$	1267[39–41,43]	1216, 1162[59–61]	1185[39]	1220, 1143[39]
	$\nu_{as}(NH_3)$	3344[40,41,43]	3395, 3347[59–61]	3391, 3364[42,59–61]	
	$\nu_s(NH_3)$	3201[40,41,43]	3245, 3139[59–61]	3257, 3198[42,59–61]	3212[42,43,59–61]
B-acid sites	$\delta_s(NH_4^+)$	1697[39–41]	1481, 1460[59–61]		
	$\delta_{as}(NH_4^+)$	1461[39–41]			1434[39–41]
	$\nu(NH_4^+)$	3031, 2784[42,43]	3024, 2780[59–61]	3024, 2788[42,43]	3036, 2842[39–41]

Published on 27 November 2015. Downloaded by RESEARCH CENTRE FOR ECO-ENVIRONMENTAL SCIENCES, CAS on 23/02/2016 08:39:49.

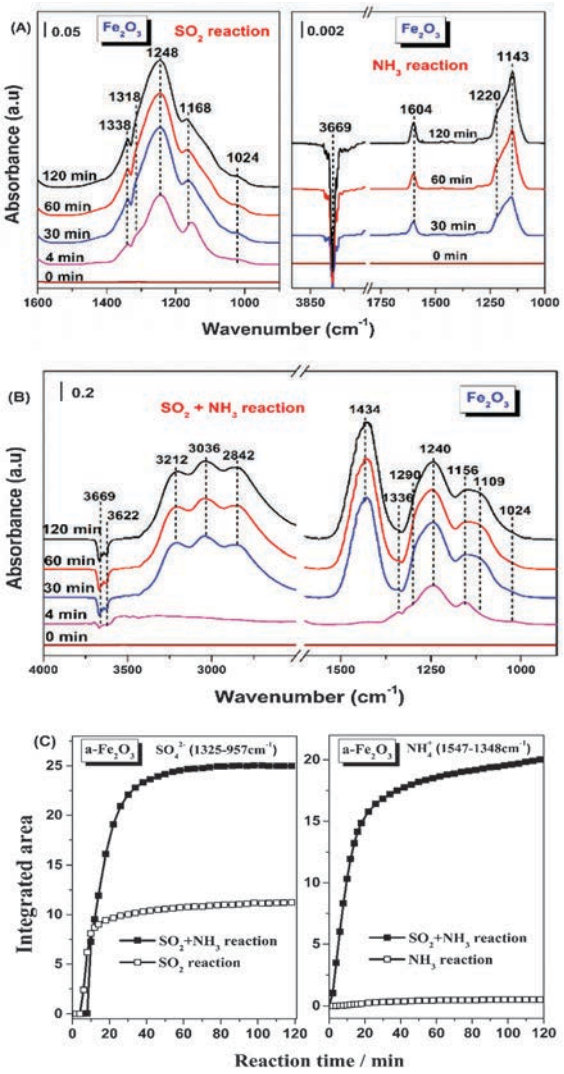

Fig. 6 *In situ* DRIFTS spectra of α-Fe_2O_3 exposed to (A) individual 200 ppmv SO_2 or 100 ppm NH_3, (B) 200 ppmv SO_2 and 100 ppmv NH_3 simultaneously, and (C) integrated areas of sulfate and ammonium under those two conditions.

free sulfate ions at 1100 cm^{-1} in a weak base solution of Na_2SO_4 *via* ATR-FTIR, and found that the band would be split into bands at 1210 and 1045 cm^{-1} once the pH is decreased.[62] In the present study, the increased intensity of the band at 1109 cm^{-1} indicated that the surface basicity increased with co-adsorption of NH_3, and that the adsorbed sulfate species may undergo chemical changes to become low-coordinated sulfate species. The bands at 1318, 1248 and 1165 cm^{-1} red-shifted to lower frequencies at 1290, 1240 and 1156 cm^{-1} attributed to bridging sulfate, implying that sulfate species tend to change from bidentate to monodentate.[47,55,58] Adsorbed NH_3 species also underwent chemical changes in the presence of SO_2 because new bands corresponding to NH_4^+ species on Brønsted acid sites appeared.[40,42] Similar to other oxides, integrated areas (Fig. 6(C)) confirmed a synergistic effect between SO_2 and NH_3 on α-Fe_2O_3, indicating that the mechanism of synergistic reactions on different mineral oxides may be identical.

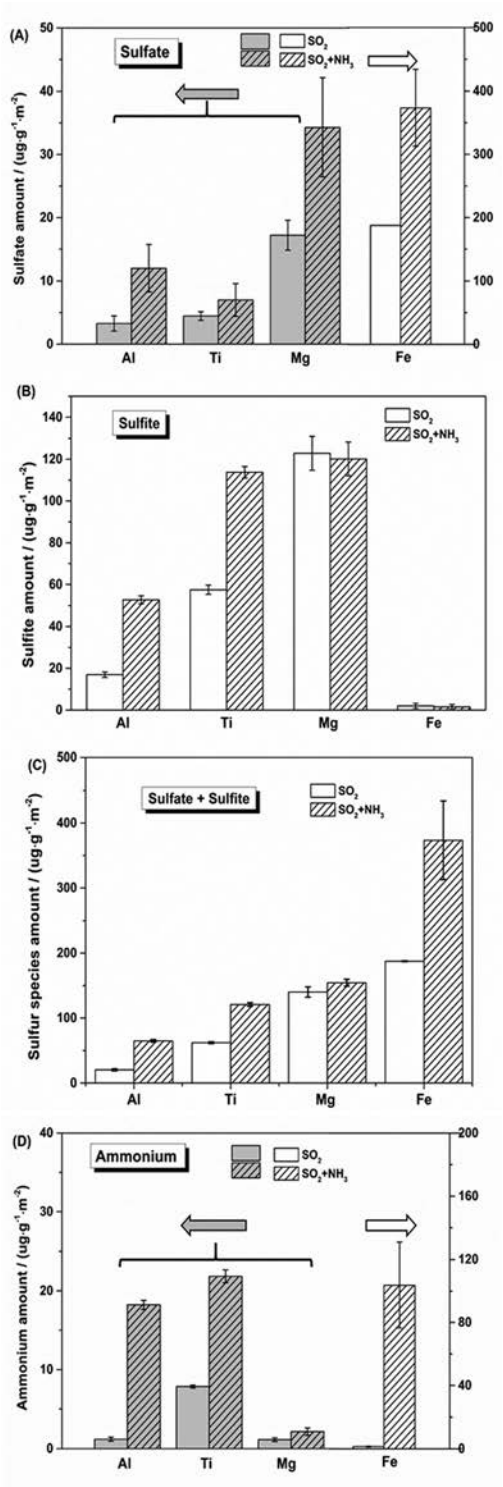

Fig. 7 Ion chromatography results of the amounts of (A) sulfate, (B) sulfite, (C) sulfate + sulfite, and (D) ammonia species (product per unit mass/surface area of the sample) formed on the surfaces of oxides after reaction with SO_2 and SO_2 + NH_3.

It is known that *in situ* DRIFTS and XPS are only surface-sensitive and poor in terms of quantitative analysis. Therefore, ion chromatography (IC) was used to investigate the reaction

 This journal is © the Owner Societies 2016

Published on 27 November 2015. Downloaded by RESEARCH CENTRE FOR ECO-ENVIRONMENTAL SCIENCES, CAS on 23/02/2016 08:39:49.

products of SO_2 and NH_3 formed on mineral dust quantitatively as shown in Fig. 7. The oxide powders were placed in a fixed bed quartz tube reactor and treated with SO_2 or/and NH_3 for 60 min. The reaction conditions were the same as those for *in situ* DRIFTS. It was found that the formation of sulfur species was significantly promoted by NH_3. For MgO and α-Fe_2O_3, the promotion function by NH_3 was obvious for sulfate species while nearly no effect was found for sulfite species. In contrast, sulfite species was obviously promoted to form on γ-Al_2O_3 and TiO_2. And a weaker promotion effect was detected for sulfate species. Fig. 7(C) shows the total sulfur species formed on mineral dust under different reaction conditions and the enhancing multiple by NH_3 decreased in the order of γ-Al_2O_3 (3.20) > α-Fe_2O_3 (1.99) > TiO_2 (1.94) > MgO (1.10). In the case of NH_3 species (Fig. 7(D)), the promotion effect by SO_2 was also more significant for acidic oxides like γ-Al_2O_3 and α-Fe_2O_3 compared to basic oxides like MgO. It was noted that the amount of NH_4^+ given here was the total amount of ammonia adsorbed on mineral dust. Similar to the DRIFTS results, the IC results confirmed that a synergistic effect between SO_2 and NH_3 existed on mineral dust. Table S2 (ESI†) shows the IC results of reacted α-Fe_2O_3 after exposure to SO_2 or/and NH_3 for different times in the *in situ* chamber, and it was found that the adsorption of SO_2 and NH_3 was promoted by each other, indicating that the synergistic effect can be reproducible in the *in situ* chamber.

Mechanism for SO_2 reaction on mineral dust

Sulfite-like species were produced when SO_2 interacted with γ-Al_2O_3, TiO_2, and MgO at room temperature. Previous studies elaborated the mechanism for the adsorption of SO_2 on oxides involving initial adsorption of SO_2 either on Lewis acid sites (coordinately unsaturated aluminum atoms) to form weakly adsorbed SO_2 or on Lewis base sites (exposed oxygen atoms) followed by rearrangement to form chemisorbed sulfite *via* the following surface reaction:[38]

$$SO_2 + O_{(lattice)}^{2-} \rightarrow SO_3^{2-}\,(a) \quad (1)$$

The result was confirmed by a theoretical study that the formation of surface sulfite was favored when SO_2 interacted with low-coordinated O^{2-} at steps and kinks.[63]

Surface hydroxyls were the principal reactive sites on metal oxides, which functioned as adsorption sites for water and in turn, adsorbed water dissociated into more hydroxyls at oxygen vacancies or hydrogen-bonded to surface O–H groups.[64–66] Zhang *et al.* proposed that those metal oxides having empty or half-empty d atom orbitals, such as Al_2O_3, tend to adsorb O_2 and H_2O (g) to form surface hydroxyls, which are in favor for the heterogeneous reaction with SO_2.[18] Accordingly, for highly hydroxylated oxides, such as TiO_2 and Al_2O_3, sulfite species also formed according to reactions (2) and (3):[15,16]

$$SO_2 + OH^-\,(a) \rightarrow HSO_3^{2-}\,(a) \quad (2)$$

$$SO_2 + 2OH^-\,(a) \rightarrow SO_3^{2-}\,(a) + H_2O \quad (3)$$

In addition to sulfite, sulfate species formed on the surface of γ-Al_2O_3, TiO_2 and MgO. To date, a few studies have observed the oxidation of SO_2 on the surface of Al_2O_3 and TiO_2 at room temperature without other oxidants.[15,50] Baltrusaitis *et al.* stated that surface oxygen atoms interacted with adsorbed SO_3^{2-} species on Al_2O_3 to withdraw the electron density from the sulfur atom and generated a "sulfate-like" species without electron transfer taking place.[17] Smith *et al.* compared the reactions of SO_2 with nearly perfect and high-defect TiO_2(110) surfaces and found that SO_2 reacted vigorously with defects while interacted weakly with nearly perfect TiO_2(110).[67] Warburton *et al.* identified the conversion of sulfite species to sulfate through incorporation into two raised-row O atoms on TiO_2(110) using NEXAFS.[68] Noting that lots of defects and step edges exist on oxide particles (*e.g.* TiO_2, Fig. S5, ESI†) and the reactivity in the formation of sulfate decreased for calcined-TiO_2 due to restored defects (Fig. S6, ESI†), it is found that the oxide powders used in this study provide favorable sites for the reaction between SO_3^{2-} and oxygen atoms. A reaction for sulfate formation has been proposed as shown in eqn (4).[17] $[O]_{(surface)}$ here represents the oxygen species on the surface of the sample.

$$SO_3^{2-}\,(a) + [O]_{(surface)} \rightarrow SO_4^{2-}\,(a) \quad (4)$$

In this study, a clear growth of the band at 1623 cm^{-1} with increasing time was observed when γ-Al_2O_3 was exposed to SO_2 (Fig. 1). The band at 1623 cm^{-1} was assigned to the bending mode of the adsorbed H_2O.[69] Though the formation of SO_3^{2-} was involved in the generation of H_2O, it was proposed that the formation of SO_4^{2-} was also accompanied by the generation of H_2O as shown below:[18,50]

$$HSO_3^-\,(a) + [O]_{(surface)} + OH^-\,(a) \rightarrow SO_4^{2-}\,(a) + H_2O \quad (5)$$

The formation pathway of SO_4^{2-} on α-Fe_2O_3 is likely different relative to γ-Al_2O_3 and MgO, because Fe(III) in α-Fe_2O_3 is much more active in the oxidation of SO_2 to sulfate. As shown in the DRIFTS spectra, surface-coordinated sulfate or bisulfate species dominated on the surface of α-Fe_2O_3. Several previous studies found that a redox process took place in the heterogeneous reaction of SO_2 on Fe(III), containing aerosols, where Fe(III) could be reduced to Fe(II) by oxidizing low-valence sulfur compounds like SO_2.[16,70] Fu *et al.* proposed that oxygen was involved in the re-oxidation of Fe(II) to Fe(III) through reaction with $SO_3^{\bullet-}$ during this process.[16] The reactions could be expressed:

$$Fe(III) + OH^-\,(a) + HSO_3^- \rightarrow Fe(II) + SO_3^{\bullet-}\,(a) + H_2O \quad (6)$$

$$Fe(II) + SO_3^{\bullet-}\,(a) + [O]_{(surface)} \rightarrow Fe(III) + SO_4^{2-}\,(a) \quad (7)$$

These reactions only proceed on an acidic surface, for example, when SO_2 reacts alone on α-Fe_2O_3. However, in this study, the presence of NH_3 increased the basicity of α-Fe_2O_3, thus a different reaction may occur when the sample is exposed to SO_2 and NH_3 simultaneously. Baltrusaitis *et al.* proposed an alternative mechanism for the oxidation of SO_2 to sulfate involving the reaction of adsorbed sulfite with activated molecular oxygen at α-Fe_2O_3 oxygen vacancy sites.[17] The reactions are as follows:

$$O_{(vacancy)} + O_{2(g)} + 2e^- \rightarrow 2O^- \quad (8)$$

$$SO_3^{2-}\,(a) + O^- \rightarrow SO_4^{2-}\,(a) + e^- \quad (9)$$

Published on 27 November 2015. Downloaded by RESEARCH CENTRE FOR ECO-ENVIRONMENTAL SCIENCES, CAS on 23/02/2016 08:39:49.

As α-Fe_2O_3 was in fact oxygen deficient and NH_3 is a good electron-pair donor, Fe–O (vacancy) was a negatively charged oxygen vacancy.[17,71] Therefore, the heterogeneous reactions of SO_2 on α-Fe_2O_3 may also take place in this way.

Mechanism of NH_3 promotion for the formation of sulfate species

In the present study, the presence of NH_3 promoted the formation of sulfite and sulfate species obviously, especially on hydroxylated oxides like α-Fe_2O_3 and γ-Al_2O_3. Early studies proposed that the water film on the surface of vessels was responsible for the fast oxidation of SO_2 to sulfate in the presence of NH_3.[31,32] Even though this study was conducted under dry conditions, gaseous water molecules would be present and adsorbed on the surfaces of oxides. Under these conditions, NH_3 would "dissolve in" water by producing NH_4^+ *via* reaction (10) or bond to water molecules through a hydrogen bond between the H atom of H_2O and the N atom of NH_3.[72–74]

$$NH_3 + H_2O\ (a) \rightarrow NH_4^+\ (a) + OH^-\ (a) \qquad (10)$$

The FTIR result suggested that this reaction occurs readily on γ-Al_2O_3 and TiO_2 (Fig. 1(B) and Fig. S3(A), ESI†). The increased surface basicity due to the generation of OH^- *via* eqn (10) would promote the adsorption of SO_2 as HSO_3^- or SO_3^{2-} *via* reactions (2) and (3), and a homogeneous-like process consisting of oxidation of HSO_3^- or SO_3^{2-} to SO_4^{2-} in the presence of oxygen may be involved in the formation of sulfate species.[75] Since oxygen vacancy sites and acid–base properties of the hydroxyl groups on solid oxides determine the chemical properties of the oxides, NH_3 may also promote the formation of sulfate in other ways.[33,34] It was found that the adsorption of NH_3 coordinatively on Lewis acid sites was obvious for TiO_2 and α-Fe_2O_3 (Fig. S3(A), ESI† and Fig. 6(A)), possibly due to considerable oxygen vacancies near the surface of TiO_2 and α-Fe_2O_3.[71,76] Besides, hydroxyl groups were clearly consumed when NH_3 interacted with mineral dust, suggesting that surface acid hydroxyls act as adsorption sites for NH_3.

When NH_3 adsorbed on the surfaces of oxides, a synergistic adsorption of SO_2 may occur as SO_3^{2-} *via* reactions (1)–(3). Since SO_3^{2-} is a strong proton acceptor and NH_4^+ is a good proton donor, a donor–acceptor complex "^+H_4N–SO_3^{2-}" would form. The proton-transfer action between sulfite and adsorbed NH_4^+ species may stabilize the sulfite species on the surface and further oxidation of sulfite species proceeds according to reactions (4)–(9).

Mechanism of SO_2 promotion for the formation of NH_4^+

Since S=O has strong affinity to electrons, the Lewis acid strength of metal ions would become much stronger when connected to sulfate. Thus Brønsted acid sites will be created when a water molecule is bound to the Lewis acid site *via* reaction (11).[77]

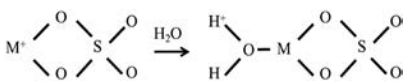

(11)

In addition, a structure resembling $(M_3O_3)S{=}O$ in the anhydrous environment or in the absence of OH groups would convert to $(M_2O_2)S{=}OOH$ in the presence of H_2O or surface OH groups, and new Brønsted acid sites would be produced in this way.[58]

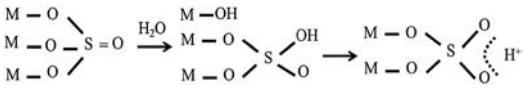

(12)

The FTIR results (*e.g.* Fig. 1) showed that NH_3 coordinated on Lewis acid sites transformed into NH_4^+ on Brønsted acid sites rapidly once the sulfate species formed. The results indicated that the increased Brønsted acid sites promoted the formation of NH_4^+ species on mineral dust.

Conclusions and atmospheric implications

A synergistic effect existed between SO_2 and NH_3 on typical mineral dust at ambient temperature was observed using *in situ* DRIFTS, and that effect was further confirmed by XPS and ion chromatography. It was found that the presence of NH_3 promoted the formation of sulfur species significantly on the surfaces of mineral oxides. Once upon sulfation, excessive Brønsted acid sites generated in the presence of water molecules which was in favor of the formation of NH_4^+. The surface properties of dust were shown to play an important role in the synergistic effect between SO_2 and NH_3.

The results have implications for atmospheric processes involving SO_2 and NH_3 on mineral dust. The metal oxides in mineral dust under solar UV light may act as atmospheric photocatalysts promoting the formation of OH radicals, initiating the conversion of SO_2 to sulfuric acid and further production of particle sulfate as reported by Dupart *et al.*[78] Whereas the reactions of SO_2 on metal oxides in the presence of NH_3 or not in the current study proceed under dark conditions, possibly thermochemical. Such reactions may occur at night only, although the importance of this dark transformation relative to rates of photochemical oxidation of SO_2 needs to be further investigated.

Recent studies find that sulfate species account largely for severe haze pollution in China, accompanied by the increase of mineral dust, and the severe pollution episodes are attributable to new particle formation (NPF).[24,79,80] It was observed that strong nucleation events are initiated by the strong dust events, and an occurrence of high concentrations of nano-sized particles preceded aerosol nucleation.[78,80] The smaller dust particles with average grain size varying from 10 to 35 nm in this study indicate longer residence times in the atmosphere, which may affect the chemical composition of the atmosphere through interacting with SO_2 and other atmospheric gases. It will allow the formation of a large amount of new aerosols though in principle a population of dust can inhibit NPF by acting as a sink for nucleating vapors.[78] Thus the role of size distribution regarding mineral dust in the new particle formation needs to be valued.

 This journal is © the Owner Societies 2016

Published on 27 November 2015. Downloaded by RESEARCH CENTRE FOR ECO-ENVIRONMENTAL SCIENCES, CAS on 23/02/2016 08:39:49.

Enhanced atmospheric oxidation was reported to play an important role in this process.[24,78] However, the results from this study show that the coexistence of NH_3 with SO_2 promotes the formation of sulfate on mineral dust, suggesting a different reaction pathway for SO_2 in the presence of NH_3. In haze pollution days, such reaction would be expected to occur on the surfaces of mineral oxides though the heterogeneous reaction of mixed SO_2 and NH_3 with atmospheric concentration levels on mineral dust needs to be further investigated. This process will promote the consumption of SO_2 and NH_3, and production of sulfate and ammonium. Mineral oxides coated with sulfate and ammonium can act as giant seeds for cloud droplets facilitating aqueous phase reactions of other pollutants as well as warm rain initiation in a polluted atmosphere.[81] In addition, mineral dust with the addition of secondary compounds as sulfate and ammonium species may reduce the ice nucleation ability of the mineral dust due to concealing or physicochemical modification of the fraction of ice active sites as reported by previous studies.[82,83]

Finally, the difference in the synergistic effect between SO_2 and NH_3 on various mineral oxides implies the different roles of mineral dust aerosols in the transformation reactions of SO_2 and NH_3 in the atmospheric system. We found that the oxidation amount of SO_2 per unit surface decreased in the order of Fe_2O_3 > MgO > Al_2O_3 > TiO_2 in the absence of NH_3. And sulfate species was obviously promoted to form on Fe_2O_3 and MgO while sulfite species was for Al_2O_3 and TiO_2 when NH_3 coexisted in the gas flow. In the mineral aerosol system, those dust particles containing iron and magnesium might be more effective in the conversion of SO_2 towards sulfate species in the presence of NH_3. Such a difference in oxide reactivity was possibly due to the variation in the surface properties of mineral dust as reported previously.[17] Further experimental investigations, such as the influence of oxygen species, the acid–base properties of surface hydroxyls, and the different mixed-morphologies of mineral dust, are needed to establish the relationship between mineral dust and transformation of sulfur and ammonia species.

Acknowledgements

This research was financially supported by the Strategic Priority Research Program of the Chinese Academy of Sciences (XDB05010300) and the National Natural Science Foundation of China (21407158), and special fund of the State Key Joint Laboratory of Environment Simulation and Pollution Control (14L02ESPC).

Notes and references

1 D. A. Hegg, R. Majeed, P. F. Yuen, M. B. Baker and T. V. Larson, *Geophys. Res. Lett.*, 1996, **23**, 2613–2616.
2 J. Lelieveld and J. Heintzenber, *Science*, 1992, **258**, 117–120.
3 M. Luria and H. Sievering, *Atmos. Environ., Part A*, 1991, **25**, 1489–1496.
4 O. Welz, J. D. Savee, D. L. Osborn, S. S. Vasu, C. J. Percival, D. E. Shallcross and C. A. Taatjes, *Science*, 2012, **335**, 204–207.
5 R. L. Mauldin, 3rd, T. Berndt, M. Sipila, P. Paasonen, T. Petaja, S. Kim, T. Kurten, F. Stratmann, V. M. Kerminen and M. Kulmala, *Nature*, 2012, **488**, 193–196.
6 D. R. Worsnop, M. S. Zahniser and C. E. Kolb, *J. Phys. Chem.*, 1989, **93**, 1159–1172.
7 J. Liang and M. Z. Jacobson, *J. Geophys. Res.*, 1999, **104**, 13749–13769.
8 R. Zhang, G. Wang, S. Guo, M. L. Zamora, Q. Ying, Y. Lin, W. Wang, M. Hu and Y. Wang, *Chem. Rev.*, 2015, **115**, 3803–3855.
9 P. Kasibhatla, W. L. Chameides and J. S. John, *J. Geophys. Res.*, 1997, **102**, 3737–3759.
10 A. Laskin, D. J. Gaspar, W. Wang, S. W. Hunt, J. P. Cowin, S. D. Colson and B. J. Finlayson-Pitts, *Science*, 2003, **301**, 340–344.
11 A. R. Ravishankara, *Science*, 1997, **276**, 1058–1065.
12 F. J. Dentener, G. R. Carmichael, Y. Zhang, J. Lelieveld and P. J. Crutzen, *J. Geophys. Res.*, 1996, **101**, 22869–22889.
13 A. E. M. Courtney, R. Usher and V. H. Grassian, *Chem. Rev.*, 2003, **103**, 4883–4939.
14 E. Harris, B. Sinha, V. D. Pinxteren, A. Tilgner, K. W. Fomba, J. Schneider, A. Roth, T. Gnauk, B. Fahlbusch, S. Mertes, T. Lee, J. Collett, S. Foley, S. Borrmann, P. Hoppe and H. Herrmann, *Science*, 2013, **340**, 727–730.
15 A. L. Goodman, P. Li, C. R. Usher and V. H. Grassia, *J. Phys. Chem. A*, 2001, **105**, 6109–6120.
16 H. Fu, X. Wang, H. Wu, Y. Yin and J. Chen, *J. Phys. Chem. C*, 2007, **111**, 6077–6085.
17 J. Baltrusaitis, D. M. Cwiertny and V. H. Grassian, *Phys. Chem. Chem. Phys.*, 2007, **9**, 5542–5554.
18 X. Zhang, G. Zhuang, J. Chen, Y. Wang, X. Wang, Z. An and P. Zhang, *J. Phys. Chem. B*, 2006, **110**, 12588–12596.
19 M. B. Mitchell and V. N. Sheinker, *J. Phys. Chem.*, 1996, **100**, 7550–7557.
20 C. R. Usher, H. Al-Hosney, S. Carlos-Cuellar and V. H. Grassian, *J. Geophys. Res.*, 2002, **107**, 4713–4722.
21 M. Ullerstam, R. Vogt, S. Langer and E. Ljungstrom, *Phys. Chem. Chem. Phys.*, 2002, **4**, 4694–4699.
22 Q. Ma, Y. Liu and H. He, *J. Phys. Chem. A*, 2008, **112**, 6630–6635.
23 C. Liu, Q. Ma, Y. Liu, J. Ma and H. He, *Phys. Chem. Chem. Phys.*, 2012, **14**, 1668–1676.
24 H. He, Y. Wang, Q. Ma, J. Ma, B. Chu, D. Ji, G. Tang, C. Liu, H. Zhang and J. Hao, *Sci. Rep.*, 2014, **4**, 4172–4176.
25 L. D. Kong, X. Zhao, Z. Y. Sun, Y. W. Yang, H. B. Fu, S. C. Zhang, T. T. Cheng, X. Yang, L. Wang and J. M. Chen, *Atmos. Chem. Phys.*, 2014, **14**, 9451–9467.
26 S. Reis, R. W. Pinder, M. Zhang, G. Lijie and M. A. Sutton, *Atmos. Chem. Phys.*, 2009, **9**, 7657–7677.
27 S. N. Behera and M. Sharma, *Atmos. Environ.*, 2011, **45**, 4015–4024.
28 J. Liggio, S. M. Li, A. Vlasenko, C. Stroud and P. Makar, *Environ. Sci. Technol.*, 2011, **45**, 2790–2796.

Published on 27 November 2015. Downloaded by RESEARCH CENTRE FOR ECO-ENVIRONMENTAL SCIENCES, CAS on 23/02/2016 08:39:49.

29 P. Korhonen, M. Kulmala, A. Laaksonen, Y. Viisanen, R. McGraw and J. H. Seinfeld, *J. Geophys. Res.*, 1999, **104**, 26349–26353.
30 R. Zhang, A. Khalizov, L. Wang, M. Hu and W. Xu, *Chem. Rev.*, 2012, **112**, 1957–2011.
31 A. D. A. Hansen, W. H. Benner and T. Novakov, *Atmos. Environ., Part A*, 1991, **25**, 2521–2530.
32 W. H. Benner, B. Ogorevc and T. Novakov, *Atmos. Environ., Part A*, 1992, **26**, 1713–1723.
33 E. McCaferty and J. P. Wightman, *Surf. Interface Anal.*, 1998, **26**, 549–564.
34 G. Pacchioni, *ChemPhysChem*, 2003, **4**, 1041–1047.
35 H. A. Al-Abadleh and V. H. Grassian, *Surf. Sci. Rep.*, 2003, **52**, 63–161.
36 F. Liu and H. He, *J. Phys. Chem. C*, 2010, **114**, 16929–16936.
37 C. C. Chang, *J. Catal.*, 1978, **53**, 374–385.
38 A. Datta, R. G. Cavel, R. W. Tower and Z. M. George, *J. Phys. Chem.*, 1985, **89**, 443–449.
39 W. S. Kijlstra, D. S. Brands, E. K. Poels and A. Bliek, *J. Catal.*, 1997, **171**, 208–218.
40 R. Jin, Y. Liu, Z. Wu, H. Wang and T. Gu, *Chemosphere*, 2010, **78**, 1160–1166.
41 L. Zhang and H. He, *J. Catal.*, 2009, **268**, 18–25.
42 G. Busca, *Langmuir*, 1986, **2**, 577–582.
43 M. A. Centeno, *Appl. Catal., B*, 1998, **19**, 67–73.
44 M. Y. Smirnov, A. V. Kalinkin, A. V. Pashis, A. M. Sorokin, A. S. Noskov, K. C. Kharas and V. I. Bukhtiyarov, *J. Phys. Chem. B*, 2005, **109**, 11712–11719.
45 E. Garcia-bordeje, J. Pinilla, M. Lazaro, R. Moliner and J. Fierro, *J. Catal.*, 2005, **233**, 166–175.
46 D. Peak, R. G. Ford and D. L. Sparks, *J. Colloid Interface Sci.*, 1999, **218**, 289–299.
47 S. J. Hug, *J. Colloid Interface Sci.*, 1997, **188**, 415–422.
48 H. He, J. Liu, Y. Mu, Y. Yu and M. Chen, *Environ. Sci. Technol.*, 2005, **39**, 9637–9642.
49 Q. Wu, H. Gao and H. He, *J. Phys. Chem. B*, 2006, **110**, 8320–8324.
50 C. E. Nanayakkara, J. Pettibone and V. H. Grassian, *Phys. Chem. Chem. Phys.*, 2012, **14**, 6957–6966.
51 Q. Yang, C. Xie, Z. Xu, Z. Gao and Y. Du, *J. Phys. Chem. B*, 2005, **109**, 5554–5560.
52 H. Chen, L. Kong, J. Chen and L. Wang, *Environ. Sci. Technol.*, 2007, **41**, 6484–6490.
53 H. Watanabe, C. D. Gutleben and J. e. Seto, *Solid State Ionics*, 1994, **69**, 29–35.
54 T. Sugimoto and Y. Wang, *J. Colloid Interface Sci.*, 1998, **207**, 137–149.
55 T. Yamaguchi, T. Jin and K. Tanabe, *J. Phys. Chem.*, 1986, **90**, 3148–3152.
56 M. A. Martin, J. W. Childers and R. A. Palmer, *Appl. Spectrosc.*, 1987, **41**, 120–126.
57 Y. Liu, H. He, W. Xu and Y. Yu, *J. Phys. Chem. A*, 2007, **111**, 4333–4339.
58 O. Saur, M. Bensitel, A. B. Mohammed Saad, J. C. Lavalley, C. P. Tripp and B. A. Morrow, *J. Catal.*, 1986, **99**, 104–110.
59 S. Yamazoe, T. Okumura, Y. Hitomi, T. Shishido and T. Tanaka, *J. Phys. Chem. C*, 2007, **111**, 11077–11085.
60 M. A. Centeno, I. Carrizosa and J. A. Odriozola, *Appl. Catal., B*, 2001, **29**, 307–314.
61 D. A. Pena, B. S. Uphade, E. P. Reddy and P. G. Smirniotis, *J. Phys. Chem. B*, 2004, **108**, 9927–9936.
62 P. Persson and L. Lovgren, *Geochim. Cosmochim. Acta*, 1996, **60**, 2789–2799.
63 G. Pacchioni, A. Clotet and J. M. Ricart, *Surf. Sci.*, 1994, **315**, 337–350.
64 H. A. Al-Abadleh and V. H. Grassian, *Langmuir*, 2003, **19**, 341–347.
65 T. Ishikawa, W. Y. Cai and K. Kandori, *Langmuir*, 1993, **9**, 1125–1128.
66 M. A. Henderson, W. S. Epling, C. H. F. Peden and C. L. Perkins, *J. Phys. Chem. B*, 2003, **107**, 534–545.
67 K. Smith, J. Mackay and V. Henrich, *Phys. Rev. B: Condens. Matter Mater. Phys.*, 1987, **35**, 5822–5829.
68 D. R. Warburton, D. Purdie, C. A. Muryn, K. Prabhakaran, P. L. Wincott and G. Thornton, *Surf. Sci.*, 1992, **269/270**, 305–309.
69 A. L. Goodman, E. T. Bernard and V. H. Grassian, *J. Phys. Chem. A*, 2001, **105**, 6443–6457.
70 G. Zhuang, J. Guo, H. Yuan and C. Y. Zhao, *Chin. Sci. Bull.*, 2001, **46**, 895–900.
71 O. Warschkow and D. E. Ellis, *J. Am. Ceram. Soc.*, 2002, **85**, 213–220.
72 M. A. Kebede, M. E. Varner, N. K. Scharko, R. B. Gerber and J. D. Raff, *J. Am. Chem. Soc.*, 2013, **135**, 8606–8615.
73 C. Lee, G. Fitzgerald, M. Planas and J. J. Novoa, *J. Phys. Chem.*, 1996, **100**, 7398–7404.
74 D. J. Donaldson, *J. Phys. Chem. A*, 1999, **103**, 62–70.
75 J. A. Phillips, M. Canagaratna, H. Goodfriend and K. R. Leopold, *J. Phys. Chem.*, 1995, **99**, 501–504.
76 X. Pan, M. Q. Yang, X. Fu, N. Zhang and Y. J. Xu, *Nanoscale*, 2013, **5**, 3601–3614.
77 B. Q. Jiang, Z. B. Wu, Y. Liu, S. C. Lee and W. K. Ho, *J. Phys. Chem. C*, 2010, **114**, 4961–4965.
78 Y. Dupart, S. M. King, B. Nekat, A. Nowak, A. Wiedensohler, H. Herrmann, D. Gregory, B. Thomas, A. Miffre, P. Rairoux, B. D'Anna and C. George, *Proc. Natl. Acad. Sci. U. S. A.*, 2012, **109**, 20842–20847.
79 Y. Sun, Q. Jiang, Z. Wang, P. Fu, J. Li, T. Yang and Y. Yin, *J. Geophys. Res.: Atmos.*, 2014, **119**, 4380–4398.
80 S. Guo, M. Hu, M. L. Zamora, J. Peng, D. Shang, J. Zheng, Z. Du, Z. Wu, M. Shao, L. Zeng, M. J. Molina and R. Zhang, *Proc. Natl. Acad. Sci. U. S. A.*, 2014, **111**, 17373–17378.
81 Y.-H. Zhang and C. K. Chan, *J. Phys. Chem. A*, 2002, **106**, 285–292.
82 R. C. Sullivan, M. D. Petters, P. J. DeMott, S. M. Kreidenweis, H. Wex, D. Niedermeier, S. Hartmann, T. Clauss, F. Stratmann, P. Reitz, J. Schneider and B. Sierau, *Atmos. Chem. Phys.*, 2010, **10**, 11471–11487.
83 P. Reitz, C. Spindler, T. F. Mentel, L. Poulain, H. Wex, K. Mildenberger, D. Niedermeier, S. Hartmann, T. Clauss, F. Stratmann, R. C. Sullivan, P. J. DeMott, M. D. Petters, B. Sierau and J. Schneider, *Atmos. Chem. Phys.*, 2011, **11**, 7235–7289.

 This journal is © the Owner Societies 2016